Kinetics of the lamellar and hexagonal phase transitions in phosphatidylethanolamine

Time-resolved x-ray diffraction study using a microwave-induced temperature jump

Martin Caffrey,* Richard L. Magin,‡ Bernard Hummel,* and Jian Zhang‡
*Department of Chemistry, The Ohio State University, Columbus, Ohio 43210; and ‡Bioacoustics Research Laboratory, University of Illinois, Urbana, Illinois 61801 USA

ABSTRACT The kinetics of the thermotropic lamellar gel ($L_{\beta'}$)/lamellar liquid crystal (L_α) and L_α/inverted hexagonal (H_{II}) phase transitions in fully hydrated dihexadecylphosphatidylethanolamine (DHPE) have been studied. Measurements were made by using time-resolved x-ray diffraction (TRXRD) to monitor progress of the transitions. In these studies microwave energy at 2.5 GHz was used to increase the sample temperature rapidly and uniformly through the phase transition regions. The $L_{\beta'}/L_\alpha$ and L_α/H_{II} transitions of DHPE were examined under active microwave heating and passive cooling. The transitions were found to be repeatable and reversible, and to have an upper bound on the time required to complete the transition of <3 s. Regardless of the direction of the transition, both phase transitions appeared to be two-state with no accumulation of intermediates to within the sensitivity limits of the TRXRD method. The rate and amplitude of the temperature jump can be controlled by regulating microwave radiation input power. A temperature jump rate of 29°C/s was obtained at a final microwave power setting of 120 W. Comparisons between previously reported fluid flow (Caffrey, M. 1985. *Biochemistry.* 24:4826–4844) and microwave heating studies suggest that the determination of limiting transit times will require faster heating.

INTRODUCTION

Membrane fusion and lipid digestion are examples of vital physiological processes which must involve, if only locally and transiently, changes in lipid mesomorphic or phase state. To have physiological relevance, such changes must occur on a time scale comparable with those taking place in vivo. This serves to highlight the need for establishing the kinetics, and by extension, the mechanism of lipid phase transitions. Such information is integral to our understanding of the structural and compositional requirements for transitions that occur in biological, model, and reconstituted membranes, and in formulated systems. Ultimately, we seek an understanding of the mechanism of phase transitions, the structural interrelationships of the different mesomorphs, and the full range of physiological roles played by lipids.

The measurement of bulk lipid phase transition kinetics and mechanism is possible through use of time-resolved x-ray diffraction (TRXRD)[1] (Caffrey, 1989*a*; Gruner, 1987; Laggner, 1988). The advantage of this method is that the relative amounts of the interconverting phases can be measured directly and quantitatively and that individual phases can be structurally characterized during the transformation process.

To date, the most extensively used trigger in phase transition kinetic studies has been temperature (Caffrey, 1989). Temperature-jump can be effected by resistance (Joule) and laser heating and through the use of temperature-regulated fluid streams. In each case, heat transfer should be rapid and uniform throughout the sample. Measurements and calculations show that heat transfer can be limiting and can result in sizeable thermal lags and gradients in the sample (Caffrey, 1985; Gruner, 1987).

One possible way of overcoming the conductive heat transfer problem is to use microwave radiation on homogeneous, water-containing samples. Because microwaves deposit heat within the sample, a temperature jump effected in this way should be uniform and fast. Herein, lies the focus of the present study. Microwave heating was used in conjunction with TRXRD to establish the kinetics of the thermotropic lamellar gel ($L_{\beta'}$)/lamellar liquid crystal (L_α) and L_α/inverted hexagonal (H_{II}) phase tran-

[1] *Abbreviations used in this paper: c*, concentration; *C*, capacitance; CHESS, Cornell High Energy Synchrotron Source; DHPE, dihexadecylphosphatidylethanolamine; DPPC, dipalmitoylphosphatidylcholine; DPPG, dipalmitoylphosphatidylglycerol; E_m, electric field intensity; H_{II}, inverted hexagonal phase; Hepes, 4-(2-hydroxyethyl)-1-piperazineethanesulfonic acid; *K*, thermal diffusivity; L, position along the long-axis of the x-ray capillary; L_α, lamellar liquid crystal phase; $L_{\beta'}$, lamellar gel phase with tilted chains; MED, microwave exposure device; *P*, microwave power input; *q*, heating rate; TRXRD, time-resolved x-ray diffraction; t_T, transit time; Z_o, impedance of free space; Z_{TE}, waveguide impedance; ρ, density; τ, thermal time constant of Luxtron temperature sensor; υ, surface thermal conductivity; λ_o, wavelength in free space.

0006-3495/90/07/21/09 $2.00

sitions in fully hydrated dihexadecylphosphatidylethanolamine (DHPE). The results show that microwaves can be used to effect thermotropic phase transitions. Heating transit times of <3 s were recorded for the lamellar and hexagonal phase transitions at the maximum irradiated power of 120 W corresponding to a sample heating rate of 29°C/s. As was observed with fluid flow experiments, both transitions appear to be two-state with no detectable accumulation of intermediates. Despite the advantages of microwave heating for this particular pair of transitions the supply of heat required to effect the transition appears to be rate limiting.

MATERIALS AND METHODS

Materials

DHPE, obtained from Fluka Chemical Corp. (Hauppauge, NY), was judged ≥ 98% pure by thin-layer chromatography as previously described (Caffrey and Feigenson, 1981) and was used without further purification. Water was obtained from a Milli-Q water purification system (Millipore Corp., Bedford, MA). All other solvents and chemicals used were of reagent grade.

Sample preparation

Fully hydrated samples of DHPE in thin-walled (10-μm) glass or quartz capillaries (1-mm internal diameter, Charles Co., S. Natick, MA) were prepared in excess 0.1 M Hepes, pH 7.0, as previously described (Caffrey, 1985) with the exception that capillaries were left unsealed to provide access for the microwave-compatible temperature sensor (type LIA, Luxtron Corp., Mountain View, CA). The sensor, connected to a Luxtron model 2000 fluoroptic thermometer (operating at one temperature reading per second), consisted of a 1-mm diameter optical fiber with a temperature-sensitive mixture of rare earth phosphors deposited in a thin layer at its tip (Wickersheim and Alves, 1979). The sensor tip was immersed in the DHPE/water sample as close to the position of the x-ray beam as possible. However, due to variability in the capillary bore along its length, the relative position of sensor and x-ray beam varied between samples. At no time was the sensor sealed in the capillary.

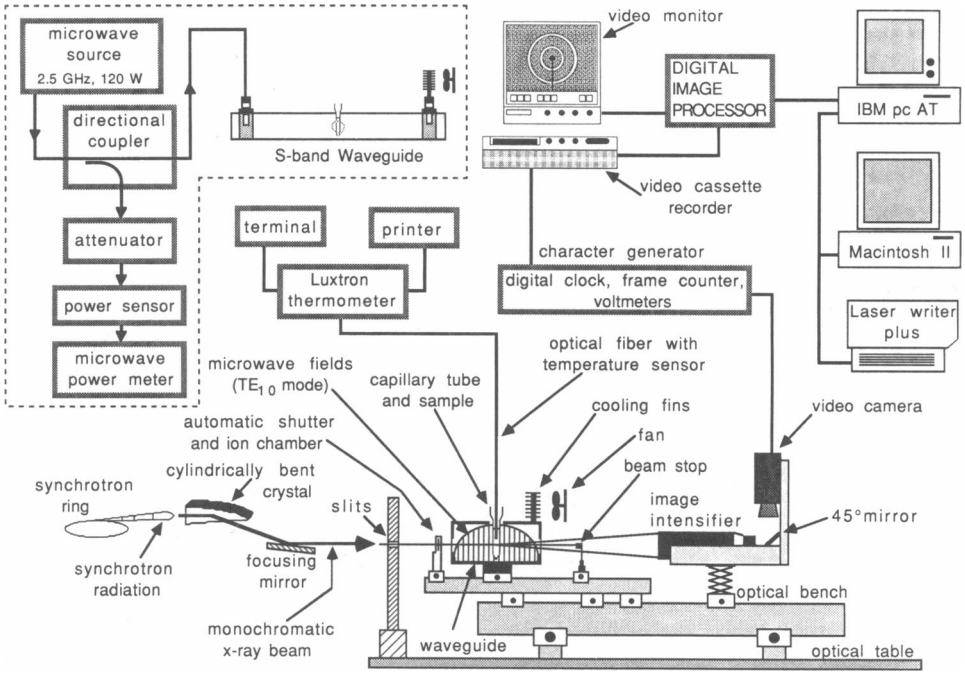

FIGURE 1 Schematic diagram of the experimental arrangement for monitoring x-ray diffraction in live time using synchrotron radiation (not drawn to scale). White radiation from the synchrotron is simultaneously monochromatized (λ = 1.57 Å, 7.9 keV) and horizontally focused by a 10 cm long, cylindrically bent germanium or silicon crystal. Higher order harmonic contaminants ($\lambda/3$, etc.) are eliminated and the 7.9 keV beam is reflected and vertically focused by a 60 cm long nickel- or platinum-coated mirror. The monochromatic beam is focused to a point 1.5 mm wide × 0.3 mm high. X-Rays diffracted from the sample are allowed to strike the fluorescent screen of a three-stage intensifier tube used for image intensification. The image is displayed dynamically on the intensifier tube and recorded using a video camera, a 45° front surfaced mirror, and a video cassette recorder. Lipid samples in glass or quartz capillaries are positioned at the center of the microwave exposure device (S-band rectangular waveguide) with a microwave compatible fiber optic based temperature sensor (Luxtron Corp., model 2000) placed in the sample as close to the x-ray beam as possible. Along with the two-dimensional diffraction image, the experiment number and elapsed time in seconds and frame number are recorded simultaneously on video tape. Data analysis is performed using a digital image processor under computer control. Inset shows the microwave power source and sensor and an alternative view of the microwave exposure device. The E-field intensity profile in the microwave exposure device is indicated by a series of vertical lines centered about the sample.

X-Ray diffraction

X-Ray diffraction measurements were carried out by using wiggler-enhanced, monochromatic (0.157-nm), focused x-rays on the A1 line at the Cornell High Energy Synchrotron Source (CHESS) as previously described (Caffrey, 1987). The machine was operating at 5.2 GeV and 20–50 mA total electron beam current in the seven-bunch mode and with the six-pole wiggler at half power.

Static and time-resolved x-ray diffraction measurements were made using a homebuilt, low-angle x-ray diffraction camera (Fig. 1) as previously described (Caffrey, 1987).

Data analysis

The video-recorded data is quantitated by digital image processing (Trapix 55/48, Recognition Concepts, Inc., Carson City, NV) using a combination of commercial (RTIPS, Tau Corp., Dayton, OH) and home-written software. Sequential digitized images or parts thereof are "grabbed" and stored in the memory of the image processor. Preliminary processing such as frame and/or circular averaging is performed on the image processor under microcomputer control. The data is then ported to a MacIntosh II computer where it is further processed to resolve composite images. An example of a digitized image of coexisting L_α and H_{II} phases is presented in Fig. 2 *A* along with the corresponding radial scan (incorporating a 20° circular averaging, 10° on either side of the indicated radius), and the resolved components consisting of, at most, two gaussians and a constant (solid lines in Fig. 2, *B* and *C*). The goodness of fit between the simulated and experimental data is shown as "error" in Fig. 2 *D* and represents the numerical difference between the experimental and the fitted function. Fits are adjusted to minimize the error. The fitted function $f(x)$ takes the form

$$f(x) = M_1 \exp\left[\frac{(x-\beta_1)^2}{\epsilon_1}\right] + M_2 \exp\left[\frac{(x-\beta_2)^2}{\epsilon_2}\right] + D,$$

where M is peak height, β is peak position, ϵ is peak width at half-height, D is a constant, and subscripts 1 and 2 refer to the first and second phase components. Peak area, A, is calculated as

$$A = k\epsilon M,$$

where k corresponds to the proportionality constant $\pi^{1/2}$ (Mencke, A. P., and M. Caffrey, manuscript in preparation).

Microwave exposure device (MED)

The MED consists of a hollow rectangular piece of aluminum waveguide (WR-284) with internal dimensions of 43.2 × 7.2 × 3.4 cm. and with a wall thickness of 2 mm. The waveguide section was modified to provide an access and positioning port for the sample. For this purpose 3-mm diameter holes were drilled and tapped on the top and bottom of the waveguide. In the holes were threaded hollow Teflon inserts that provided vertical support and positioning of the x-ray capillary to within ±2 mm of the center of the waveguide. In addition, holes of 1 mm and 2.8 cm diameter were machined through the side walls of the waveguide to accommodate the incident and diffracted x-ray beams, respectively. To maintain electrical continuity of the waveguide sidewalls, the exit port was covered with 25-μm-thick aluminum foil. This ensures the flow of surface currents because the skin depth in aluminum for the penetration of an electric field at 2.45 GHz is ~1 μm.

Thermal equilibrium measurements were performed by setting microwave power to a given level and allowing the sample to reach thermal equilibrium (usually within 2 min) before recording the diffraction pattern.

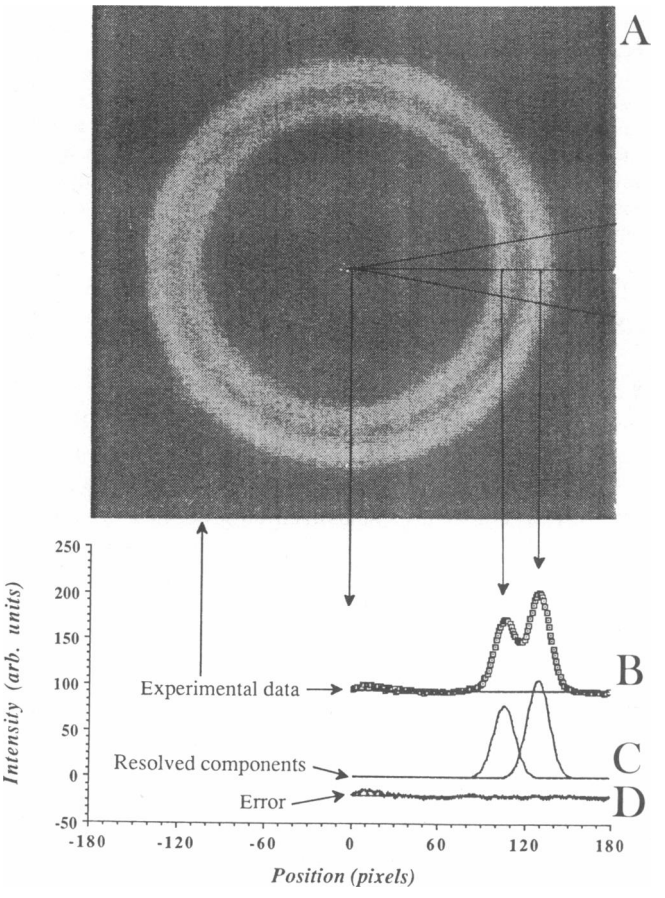

FIGURE 2 Low-angle x-ray diffraction corresponding to the L_α/H_{II} phase coexistence region in fully hydrated dihexadecylphosphatidylethanolamine observed upon heating after a 4-Watt microwave-induced temperature jump. The image corresponds to a single frame (33 ms) obtained by digital image processing (*A*). The sector indicates the 20° arc in which radial averaging is performed and which gives rise to the experimental profile presented in *B*. Raw data is fit with the sum of two gaussians and a constant indicated as solid lines in *B* and *C*. The difference (error) between observed and calculated intensity along the profile is shown in *D*.

Assuming that the sample is composed entirely of water, basic electromagnetic theory predicts a heating rate, $\dot{q}$, of 0.4°C/s for a microwave power input of 1 W. This is based on the relationship

$$\dot{q} = \left(\frac{\Delta T}{\Delta t}\right)_{1\,W} = \frac{\sigma E_m^2}{2\rho c},$$

where σ = 2.8 mho/m, c = 4.18 J/g °C, ρ = 1 g/cm^3, and E_m^2 = 121.3 V^2/cm^2 for a power input, P, of 1 W. For this calculation, the dominant TE_{10} waveguide mode of propagation is assumed so that

$$E_m^2 = \frac{4Z_{TE}P}{a\,b} = \frac{4P\left(\frac{2\pi}{\lambda_o}\right)Z_o}{ab\sqrt{\left(\frac{2\pi}{\lambda_o}\right)^2 - \left(\frac{\pi}{a}\right)^2}},$$

where λ_0 = 12.25 cm, a = 7.2 cm, b = 3.4 cm, and Z_0 = 377 Ω. Preliminary calibration studies were made using the 1-mm diameter Luxtron probe to measure the heating rate in a water-filled 1-mm quartz capillary. Heating rates of 0.41 and 1.37°C/s were obtained for net power inputs of 1.0 and 2.96 W, respectively. These experimental values correspond to heating rates of 0.41 and 0.46°C/s per Watt of input power, respectively, and agree well with theory. The heating rates observed with lipid samples were a factor of two lower than theory reflecting the high lipid content of the samples.

RESULTS

The kinetic measurements described below concern thermotropic phase transitions undergone by DHPE dispersed in excess aqueous buffer. The transitions include the $L_{\beta'}$ and L_α and L_α and H_{II} phases. It is emphasized that throughout these measurements heating was active in the sense that sample temperature was caused to rise by continuous microwave exposure. In contrast, cooling was passive, occurring in *still* air when the microwave source was turned off.

In-sample temperature was monitored continuously throughout the heating and cooling cycles by using a temperature sensor positioned inside the capillary as close to the x-ray beam as possible. A typical heating and cooling curve showing in-sample temperature at the sensor versus elapsed time after a jump in temperature from ambient (~25°C) to 75°C at an irradiated power of 5 W is presented in Fig. 3. Of interest is the absence of a pronounced thermal halt at the $L_{\beta'}/L_\alpha$ transition as was observed previously for hydrated DHPE using the forced air temperature jump system (Caffrey, 1985).

It is important to note that while every attempt was made to position the temperature sensor next to the x-ray beam, in actuality the sensor and capillary sizes were such that the two were often some distance apart. This perhaps accounts for the discrepancy between sample temperature at the x-ray beam located in the center of the MED and that at the sensor (compare Figs. 3 and 5). Calculations presented below show that thermal gradients along the length of the capillary are to be expected during the course of the temperature jump. Thus, the data in the active heating region of Fig. 3 cannot be used for transition temperature determination. However, they do show that in-sample temperature can be measured under the conditions of these experiments. The average heating and initial cooling rates observed in Fig. 3 are 1.0 and 2.8°C/s, respectively. In a repeat experiment, the corresponding values were 1.4 and 2.6°C/s. Theory and experiment show heating rates of ~0.4°C/s · W for pure water samples in a similar configuration (see Methods).

The TRXRD data obtained with fully hydrated DHPE

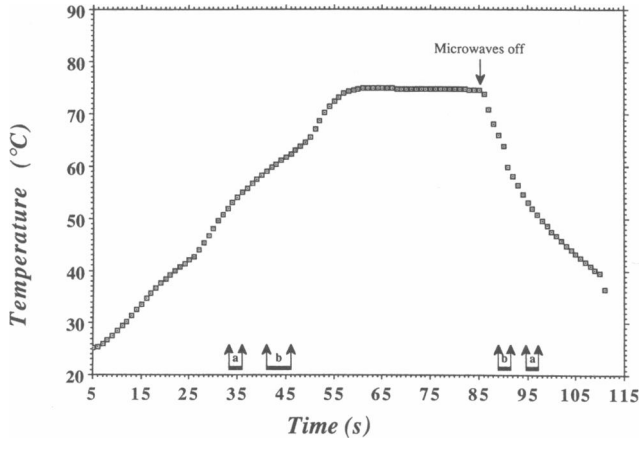

FIGURE 3 Sample temperature change with elapsed time after commencement of a 5-W microwave-induced temperature jump and passive cooling. Measurements were made with a microwave-compatible temperature sensor positioned in the fully hydrated dihexadecylphosphatidylethanolamine sample and *somewhat distant from the x-ray beam.* The range in time over which the $L_{\beta'}/L_\alpha$ (*a*) and L_α/H_{II} (*b*) phase transitions take place is indicated by the connected arrows. The average heating and initial cooling rates are 1.0 and 2.8°C/s, respectively.

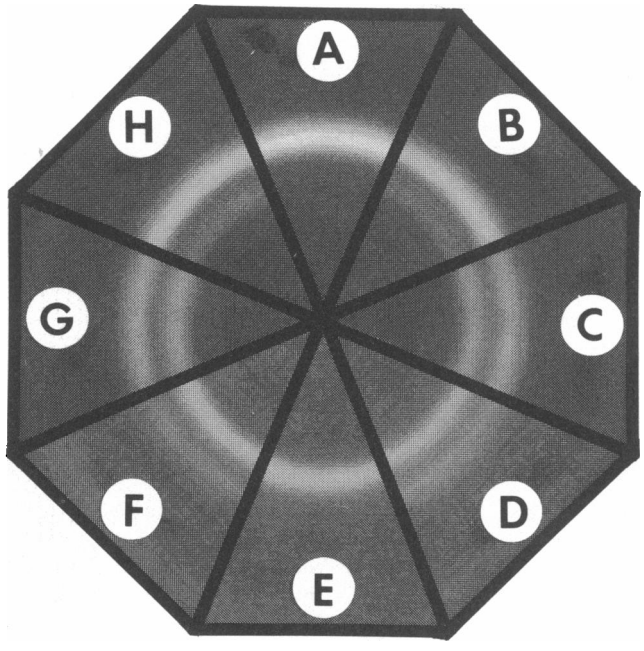

FIGURE 4 Kinetics of the lamellar liquid crystal (L_α)/inverted hexagonal (H_{II}) phase transition in fully hydrated dihexadecylphosphatidylethanolamine after a 4-W microwave-induced temperature jump and subsequent passive cooling. Low-angle x-ray diffraction corresponding to the L_α (001) and H_{II} (10) reflections was recorded by using the TRXRD method. Each sector in the composite comes from a single frame representing 33 ms of the video-recorded images. Elapsed time from the beginning of the experiment (in seconds) is (*A*) 29, (*B*) 34, (*C*) 36, (*D*) 37, (*E*) 47, (*F*) 73, (*G*) 73, and (*H*) 74. Passive cooling began at ~70 s. Pure L_α phase is seen in *A*, pure H_{II} in *E*.

are presented in Figs. 4 and 5. The original, unprocessed, two-dimensional low-angle diffraction images and how these change with time and temperature during and after an applied temperature jump are presented in Fig. 4. The quantitative low-angle diffracted intensity obtained by image processing and how this changes with time after the temperature jump is presented in Fig. 5. As outlined under Data Analysis, the diffraction data are fitted with a sum of one or two gaussians and a constant. The parameters of each gaussian, namely, peak position, height, and width at half-height, along with peak area, are included in Fig. 5. At low temperature in the vicinity of 25°C the $L_{\beta'}$ phase alone is observed as a low-angle lamellar (001) reflection. Upon heating, the total scattering angle (2θ) of the (001) reflection increases in a continuous manner. Continued heating brings about phase transformation from $L_{\beta'}$ to L_α and, over a narrow temperature range, the two phases coexist. With time and continued heating, the conversion proceeds with the intensity (peak area and height, Fig. 5 *A* and *B*) in the $L_{\beta'}$ line decreasing accompanied by a corresponding increase in the intensity of the L_α line. At the "chain melting" transition the change in 2θ is discontinuous. When the transition is complete and as sample temperature rises, the 2θ value of the L_α (001) reflection increases continuously. With increasing temperature, the first sign of the H_{II} phase becomes apparent. The intensity of the H_{II} (10) line grows at the expense of that in the L_α (001) line with continued heating until the L_α line has disappeared. As with the $L_{\beta'}/L_\alpha$ transition, the L_α/H_{II} phase change is discontinuous. Above the hexagonal transition the 2θ value of the (10) reflection increases with temperature. As expected, the L_α/H_{II} transition is less sharp than that of the $L_{\beta'}/L_\alpha$ as evidenced by phase coexistence over a larger time/temperature range (Caffrey, 1985).

The reverse process occurs when microwave radiation

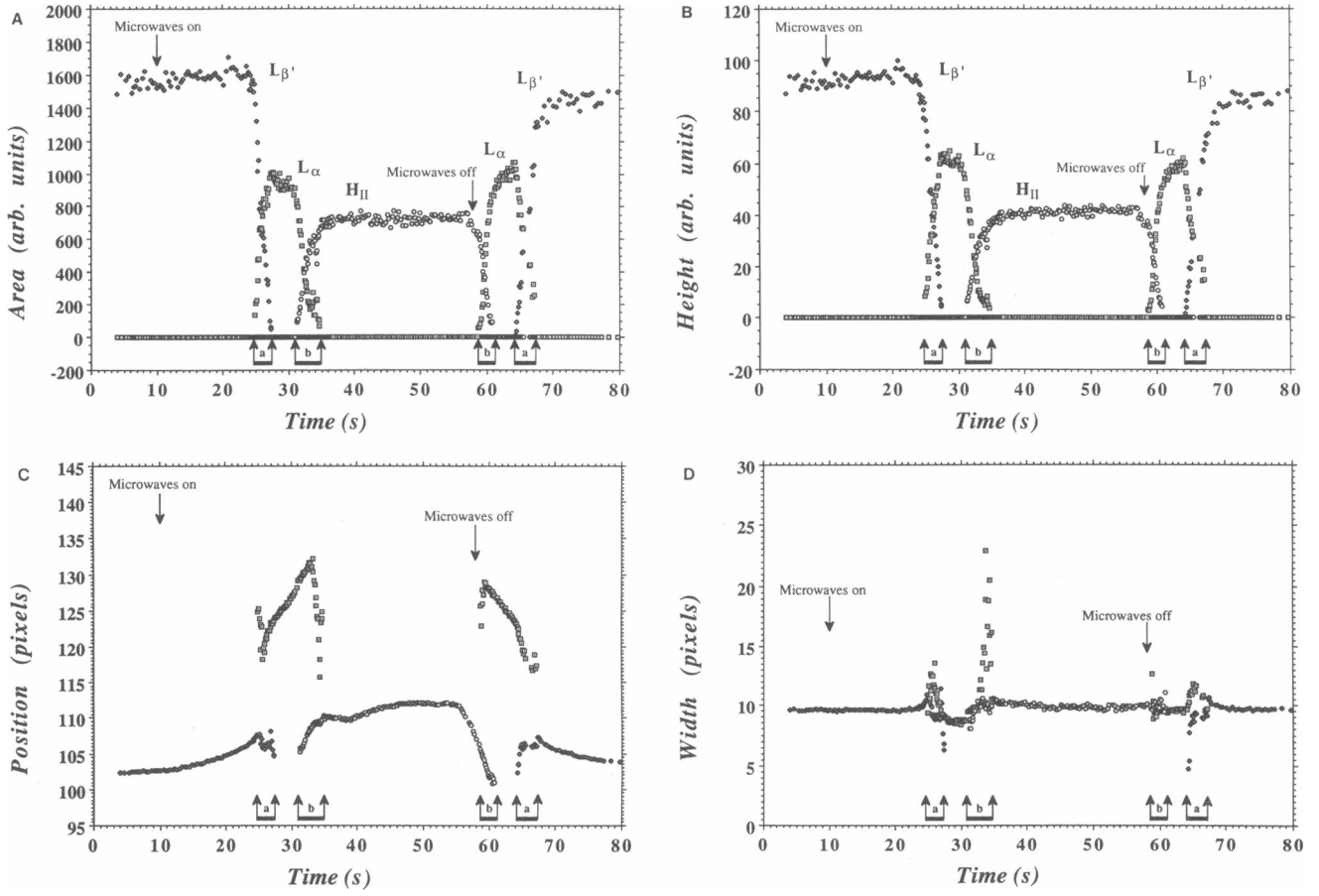

FIGURE 5 Kinetics of the phase transitions undergone by fully hydrated dihexadecylphosphatidylethanolamine in response to a 5-W microwave-induced temperature jump. Low-angle x-ray diffraction was recorded in live time and integrated intensity (area, *A*) and peak height (*B*), position (*C*), and width (*D*) were obtained by image processing as described in Data Analysis. Each data point corresponds to a single (33-ms) frame with radial averaging over a 20° arc. The point in time when microwave radiation was turned on and off is indicated. The connected arrows indicate the time interval during which phase coexistence is observed.

is turned off and sample cooling begins (Fig. 5). The process of microwave-induced heating and passive cooling was repeated many times and was found to be reproducible.

The experiment described above (Figs. 4 and 5) was performed using a microwave power setting of $\leq$ 5 W. Under these conditions, the $L_{\beta'}$ to L_α and L_α to H_{II} transitions were complete in $\leq$ 3 s and $\leq$ 5 s, respectively (Table 1). Increasing the power setting effected faster sample heating and a reduction in the time required to undergo the transition also referred to as the gross transit time (t_T, defined in footnote ‡, Table 1). Surprisingly, the cooling transitions had longer transit times at the higher microwave settings and, thus, final sample temperature.

As observed with the temperature-regulated forced air–induced temperature jump, both the lamellar and hexagonal phase transitions appear to be two-state to within the sensitivity limits of the method. This implies that at no point during the transition is there any more than two phases with no accumulation of intermediates. It is noted, however, that the method suffers from a low sensitivity to diffuse scatter. Thus, small amounts of the sample in such a form may go undetected.

The equilibrium thermotropic properties of the fully hydrated DHPE system was examined over a range of fixed microwave power inputs. The sample temperature was equilibrated at a given power setting for ~2 min and the low-angle patterns recorded by using TRXRD as for the dynamic experiments described above. This procedure was repeated over a range of temperatures encompassing both $L_{\beta'}/L_\alpha$ and L_α/H_{II} transitions. As was observed with the kinetic experiments, the temperature width (ΔT) of the hexagonal transition as judged by peak area and height was two to three times that of the lamellar order/disorder transition (data not shown). Further, transition temperatures of 52 and 62°C were recorded in the course of these equilibrium microwave heating experiments which correspond, respectively, to the 68°C and 83–86°C values reported for the $L_{\beta'}/L_\alpha$ and L_α/H_{II} transitions (Caffrey, 1985; Seddon et al., 1984). This discrepancy in transition temperatures arises, at least in part, because the temperature sensor was positioned 1–1.5 cm distant from the x-ray beam which passes through the center of the MED and because of nonuniform sample heating along the height axis of the MED and, thus, the sample capillary.

The magnitude of the aforementioned temperature gradient along the length of the sample capillary during microwave heating was estimated by considering a simple one-dimensional heat flow model. Although microwave heating (σE^2) is expected to be uniform (for the TE_{10} waveguide mode) along the length of the sample, the resulting temperature distribution is nonuniform, reflecting heat losses at the ends and surface of the sample. The appropriate differential equation and boundary conditions for this situation are given below:

$$\frac{\partial T(x,t)}{\partial t} = \kappa \frac{\partial^2 T(x,t)}{\partial x^2} - \upsilon(T - T_o) + \dot{q}$$

$$T(o,t) = T_o$$

$$T(L,t) = T_o$$

$$\kappa = K/\rho C,$$

where $T(x,t)$ is the temperature at time t and position x along the axis L of the sample capillary and T_0 is the

TABLE 1 Transit times of the thermotropic phase transitions undergone by fully hydrated dihexadecylphosphatidylethanolamine in response to microwave-induced temperature jumps

Microwave power	Fluid flow temperature jump*	Transit time‡				Reference
		$L_{\beta'} \rightarrow L_\alpha$	$L_\alpha \rightarrow H_{II}$	$H_{II} \rightarrow L_\alpha$	$L_\alpha \rightarrow L_{\beta'}$	
W	°C	*s*	*s*	*s*	*s*	
5		2.6 ± 0.4	4.6 ± 0.8	2.5 ± 0.8	3.3 ± 0.9	
100		1.8	2.0	4.0	4.0	
120		2.1	2.6	6.0	5.8	
	30 → 93	2	5	3	3	Caffrey, 1985
	30 → 126	1	1	2	3	Caffrey, 1985

Progress of the transition was monitored by low-angle time-resolved x-ray diffraction.

*Temperature jump refers to TRXRD measurements performed by using a temperature-regulated forced air stream from the indicated initial to final temperatures. They are included for comparison with the microwave data.

‡At the 5 W power setting, transit time values are reported as the mean ± SD (n = 4). Transit time refers to the time it takes to undergo the indicated phase change as judged by analysis of the image processed data of the type shown in Fig. 5 and by visual inspection of the video-recorded TRXRD images. Transit time is the time interval between the first sighting of diffraction from the newly forming phase and the last detectable diffraction from the phase undergoing the transformation. The transit times reported are gross values and include the time required to (*a*) heat/cool the sample through the transition temperature range, (*b*) supply/remove the latent heat of the transition, and (*c*) undergo the transition, i.e., the intrinsic or net transit time. Thus, the intrinsic time is always less than the measured gross value.

temperature of the surrounding air. The constants κ, K, ρ, C, υ, and $\dot{q}$ are thermal diffusivity, thermal conductivity, density, heat capacity, surface conductivity, and heating rate, respectively. The solution to this problem, provided by Carslaw and Jaeger (1986, Eq. 3, p. 159), is rewritten below as

$$T(x,t) = T_{\text{steady-state}} - \sum_{n=1}^{\infty} a_n \sin(b_n x)\, e^{-\upsilon t}\, e^{-\kappa b_n^2 t} \quad \text{(heating)}$$

$$T(x,t) = \sum_{n=1}^{\infty} a_n \sin(b_n x)\, e^{-\upsilon t}\, e^{-\kappa b_n^2 t}, \quad \text{(cooling)}$$

where

$$T_{\text{steady-state}} = \frac{\dot{q}}{\upsilon}\left[1 - \frac{\sinh\mu x + \sinh\mu(L - x)}{\sinh\mu L}\right]$$

$$a_n = \frac{4\dot{q}}{\pi\upsilon} \frac{L^2\mu^2}{(2n-1)[(2n-1)^2\pi^2 + L^2\mu^2]}$$

$$b_n = \frac{(2n-1)\pi}{L}$$

$$\mu = \sqrt{\frac{\upsilon}{K}}.$$

Values for $\dot{q}$ and υ were obtained by fitting the experimental data for heating and cooling to this equation. The value of K was estimated from steady-state temperature measurements at the center of the sample and from the thermal conductivity values of water, fat, and glass reported in Tables 3.2 and 3.3 of Sekins and Emery, 1982. Using these parameters, the temperature distribution along the sample is shown in Fig. 6 as a function of time after the application of microwave power. As the sample is heated, a temperature gradient arises along the sample. By the time a steady-state temperature distribution is reached the gradient is sufficient to account for the discrepancy in the transition temperatures noted above. Thus, for a sensor position ~1.5 cm above the center of the MED, measured temperature at the sensor tip is expected to be considerably lower than that at the center of the sample. The actual temperature differential will depend on the exact position of the sensor and the time elapsed after the application of microwave power (Fig. 6).

An added complication arises when we consider the sensor as part of the system under investigation. The sensor is a 1-mm diameter glass optical fiber which will not absorb significant amounts of microwave power. Thus, upon microwave heating it will act to retard sample heating rate as a result of conductive heat transfer. This alone may account for the apparent discrepancy between sensor temperature and that at the center of the MED. Since cooling is a passive process, such a discrepancy is expected to disappear or to be less marked as the sample and the sensor cool together at approximately the same rate.

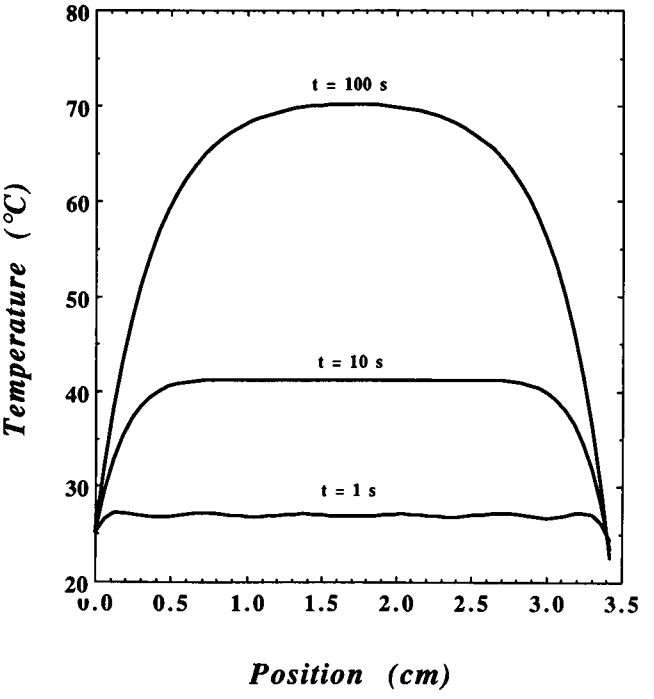

FIGURE 6 Calculated temperature distribution along the length of an x-ray capillary as a function of heating time in the microwave cavity. The ambient temperature is set at 25°C. The sample capillary is assumed to be composed entirely of water and of uniform bore (1 mm dia.) along its full length which is set equal to the height of the microwave exposure device (3.4 cm). At t = 100 s, the temperature profile approaches the steady-state distribution. The parameters used in the calculation are: $\upsilon = 3.5 \times 10^{-2}$/s; $\dot{q}$ = 0.4°C/($s \cdot W$) for P = 5 W; and K = 0.9 W/(m · °C).

DISCUSSION

The data in Table 1 suggest that as microwave power increases, the transit times of the heating transitions decrease. At the maximum power input of 120 W the $L_{\beta'}/L_{\alpha}$ and L_{α}/H_{II} transit times were 2.1 and 2.6 s, respectively. In light of the fact that the shortest corresponding values obtained using the fluid flow system were both 1 s (Caffrey, 1985), it seems unlikely that the values observed at 120 W are true limiting values. A more powerful microwave source will be required to evaluate this possibility.

The transit time values observed using microwave and fluid flow temperature jumps are comparable, suggesting, qualitatively at least, that nonthermal microwave effects on the transition kinetics are not pronounced. A more careful, parallel study will be needed to examine for more

subtle microwave effects on the kinetics and mechanism of these lipid phase transitions. In this connection, it is worthwhile noting that studies by Liburdy and Magin (1985) using a similar heating apparatus to that used in the current measurements indicated an apparent microwave-induced shift in the chain "melting" transition temperature of DPPC/DPPG liposomes.

In contrast to the microwave heating transitions, the transit times observed upon cooling appear to increase at the higher microwave power settings (Table 1). One possible explanation for this unexpected result derives from having the sample sitting in the MED in a stationary, nonflowing atmosphere. Passive cooling from a higher final sample temperature will warm the ambient atmosphere to a greater extent, thereby slowing heat loss from the sample and retarding the phase transition. Providing the MED with a temperature-controlled forced air stream directed on the sample would be useful in resolving this issue.

Two mesomorphic phase transitions, the $L_{\beta'}/L_{\alpha}$ and the L_{α}/H_{II}, have been examined in the present DHPE/water system. They differ in terms of the structural parameters that undergo change as well as the dimensionality of the mesomorph periodicity. The chain order/disorder transition does not involve a change in periodicity because both phases are periodic in one dimension. In contrast, the L_{α}/H_{II} transition requires a large topological rearrangement involving structures periodic in one and two dimensions. Regardless of this difference, both transitions are fast and can take place on a time scale of seconds. They are repeatable, reversible, and two-state to within the sensitivity limits of the method. Transition intermediates do not accumulate to significant levels or they lack long-range order so as to go undetected. Both of the transitions were discontinuous in that the low-angle diffraction patterns from the two adjacent phases were resolved and did not appear to grow continuously one from the other.

The use of microwave radiation as a trigger in temperature jump experiments offers a number of advantages over the more conventional (flowing fluid, laser, Joule, Peltier) methods. Microwaves provide internal heating which, in thin homogeneous samples positioned at the center of the MED, should be uniform throughout the sample mass and free from problems that arise from conduction. The magnitude and rate of heating for a fixed sample size can be regulated over a wide range by controlling microwave power input rate and final power setting. A set point or final sample temperature can be maintained for an indefinite period. Furthermore, no additives such as salt are needed as is the case with Joule heating.

On the negative side, however, there is the need for expensive microwave generating and monitoring equipment and microwave compatible temperature sensors and measuring devices. Also, the reproducibility of the amplitude and rate of the temperature jump depends on overall sample water content, on sample homogeneity, and on reproducibility of sample preparation. Inhomogeneities in the sample can give rise to thermal gradients and nonuniform sample heating. Microwaves are also limited to providing sample temperature-jumps in the heating direction only. Finally, the possible nonthermal effects of microwave radiation must be considered. As with all phase transformation kinetic studies, transition rate may be limited by the need to supply or remove the heat of transition. With sufficient microwave power, however, it should be possible to effect temperature jumps of reasonable amplitude within microseconds.

We thank B. W. Batterman (National Science Foundation, Grant DMR 81-12822) and the entire CHESS and MacCHESS (National Institutes of Health, Grant RR-014646) staff for their invaluable help and support. The assistance of A. P. Mencke with image processing and data reduction and interpretation is gratefully acknowledged. We also wish to thank E. C. Burdette of Labthermics Technologies, Inc., Champaign, IL, for assistance in the temperature measurements and for the loan of the Luxtron model 2000 fluoroptic thermometer that was used in these experiments.

This work was supported by a grant from the National Institutes of Health (DK 36849) and a University Exploratory Research Program award (The Procter and Gamble Co.) and a Du Pont Young Faculty Award to M. Caffrey.

Received for publication 12 December 1989 and in final form 12 February 1990.

REFERENCES

Caffrey, M. 1984. X-Radiation damage of hydrated lecithin membranes detected by real-time x-ray diffraction using wiggler-enhanced synchrotron radiation as the ionizing radiation source. *Nucl. Instrum. Methods* 222:329–338.

Caffrey, M. 1985. Kinetics and mechanism of the lamellar gel/lamellar liquid crystal and lamellar/inverted hexagonal phase transition in phosphatidylethanolamine: a real-time x-ray diffraction study using synchrotron radiation. *Biochemistry.* 24:4826–4844.

Caffrey, M. 1987. Kinetics and mechanism of transitions involving the lamellar, cubic, inverted hexagonal and fluid isotropic phase of hydrated monoacylglycerides monitored by time-resolved x-ray diffraction. *Biochemistry.* 26:6349–6363.

Caffrey, M. 1989*a*. The study of lipid phase transition kinetics by time-resolved x-ray diffraction. *Annu. Rev. Biophys. Biophys. Chem.*18:159–186.

Caffrey, M. 1989*b*. Structural, mesomorphic and time-resolved studies of biological liquid crystals and lipid membranes using synchrotron radiation. *Topics Curr. Chem.* 151:75–109.

Caffrey, M., and G. W. Feigenson. 1981. Fluorescence quenching in model membranes: the relationship between Ca^{2+}-ATPase enzyme activity and the affinity of the protein for phosphatidylcholines with different acyl chain characteristics. *Biochemistry.* 20:1949–1961.

Carslaw, H. S., and J. C. Jaeger. 1986. Conduction of Heat in Solids. 2nd ed. Clarendon Press, Oxford, UK. 510.

Gruner, S. M. 1987. Time-resolved x-ray diffraction of biological materials. *Science (Wash. DC)*. 238:305–312.

Laggner, P. 1988. X-Ray studies on biological membranes using synchrotron radiation. *Topics Curr. Chem.* 145:173–202.

Liburdy, R. P., and R. L. Magin. 1985. Microwave-stimulated drug release from liposomes. *Radiat. Res.* 103:266–275.

Seddon, J. M., G. Cevc, R. D. Kaye, and D. Marsh. 1984. X-Ray diffraction study of the polymorphism of hydrated diacyl- and dialkylphosphatidylethanolamines. *Biochemistry*. 23:2634–2644.

Sekins, K. M., and A. F. Emery. 1982. Thermal science for physical medicine. *In* Therapuetic Heat and Cold. J. F. Lehmann, editor. Williams and Williams, Baltimore, MD. 81–84.

Wickersheim, K. A., and R. B. Alves. 1979. Recent advances in optical temperature measurement. Industrial Res. Dev. 21:82–89.